Vol. 15, No. 3 (2026): 882 - 894 http://dx.doi.org/10.23960/jtepl.v15i3.882-894

JURNAL TEKNIK PERTANIAN LAMPUNG

ISSN 2302-559X (print) / 2549-0818 (online)
Journal homepage : https://jurnal.fp.unila.ac.id/index.php/JTP

Drying Kinetics of Porang (*Amorphophallus oncophyllus*) Tubers at Different Sizes and Harvest Periods Using a Lewis–Runge–Kutta Approach

Saifuddin Afif[1], Sri Rahayoe[1,✉], Eni Harmayani[2], Fertika Nur Fitriyana[1], Lisa Astiana Ghina[1]

[1] Agricultural and Biosystem Engineering Department, Faculty of Agricultural Technology, Universitas Gadjah Mada, Yogyakarta, INDONESIA

[2] Food and Agricultural Product Technology Department, Faculty of Agricultural Technology, Universitas Gadjah Mada, Yogyakarta, INDONESIA

Article History:

Received : 31 August 2025
Revised : 2 January 2026
Accepted : 3 February 2026

Keywords:

Amorphophallus oncophyllus,
Convective heat transfer coefficient,
Effective drying rate constant,
Harvest time,
Runge-Kutta 4th Order,
Tuber diameter.

Corresponding Author:
✉ srahayoe@ugm.ac.id
(Sri Rahayoe)

ABSTRACT

Porang (Amorphophallus oncophyllus) is a strategic glucomannan source for food and industrial applications, whose chip and flour quality is strongly influenced by drying performance; however, the combined effects of harvest month and tuber size on convective drying kinetics remain poorly quantified. This study estimated the convective heat transfer coefficient (h) and effective drying rate constant (k) of 7-mm porang slices using a coupled heat–mass balance framework. Tubers were classified into three size categories and dried in a 50 °C cabinet dryer across five harvest months (June–October), with continuous monitoring of air and product temperatures. The Lewis thin-layer model was solved numerically using a fourth-order Runge–Kutta method, and parameters were estimated by minimizing the mean absolute percentage error. Product temperature profiles showed rapid initial heating, a quasi-steady plateau at 43–46 °C, and a final rise, indicating dominance of the falling-rate regime. Estimated h ranged from 42 to 72 W·m^{-2}·°C^{-1} and k_p from 2.70 to 3.99 h^{-1}. Two-way ANOVA showed no significant effects of harvest month, tuber size, or their interaction ($p > 0.05$), supporting the use of effective average parameters for robust drying-process standardization and scale-up.

List of symbols used in this paper:

Symbol	Description	Symbol	Description	Symbol	Description
A	Effective surface area of the porang slice exposed to drying air (m²)	MC_{wb}	Moisture content on wet basis (kg water·kg^{-1} wet material)	n_v	Evaporative mass flux (kg·m^{-2}·s^{-1})
a_c	Effective surface area ratio of the material (m²·m^{-2})	MC_{db}	Moisture content on dry basis (kg water·kg^{-1} dry matter)	$\dot{Q}_{in}$	Rate of heat input to the system (W)
C_{pp}	Specific heat capacity of porang material (J·kg^{-1}·K^{-1})	m_w	Mass of water in the sample (kg)	$\dot{Q}_{out}$	Rate of heat output from the system (W)
C_{pa}	Specific heat capacity of drying air (J·kg^{-1}·K^{-1})	m_s	Total mass of the wet sample (kg)	s	Time step size used in the numerical integration (h)
h	Convective heat transfer coefficient (W·m^{-2}·K^{-1})	m_d	Dry mass of the sample (bone-dry basis) (kg)	T_a	Drying air temperature (°C or K)
k_p	Effective drying rate constant (h^{-1})	$\dot{m}_{in}$	Mass flow rate of inlet drying air (kg·s^{-1})	T_p	Effective surface area of the porang slice exposed to drying air (m²)
L_v	Latent heat of vaporization of water (J·kg^{-1})	$\dot{m}_{out}$	Mass flow rate of outlet drying air (kg·s^{-1})	v and g	Intermediate slope terms in RK4

1. INTRODUCTION

Porang (*Amorphophallus oncophyllus*) is a tuber crop of high economic value due to its rich glucomannan content (Cruz *et al*., 2024; Soedarjo, 2021; Wahidah *et al*., 2021). Demand for porang and glucomannan originates largely from the food, pharmaceutical, and cosmetic sectors, both domestically and internationally (Bahlawan *et al*., 2021; Novitasari *et al*., 2024; Nurkhamidah *et al*., 2024; Wahidah *et al*., 2021). High annual demand is underpinned by the crop's strong adaptability across diverse agroecosystems. In recent years, the Indonesian government has supported porang cultivation and postharvest processing through initiatives to increase production and strengthen the supply chain (Handayani *et al*., 2024; Soemantri *et al*., 2021). Despite its substantial potential, porang still faces constraints at the postharvest stage, which critically determines the quality of the final products (Hawa *et al*., 2022; Nurmianto *et al*., 2020; Setiavani *et al*., 2025). Robust postharvest processing is therefore required to ensure the quality of porang-derived products.

Fresh porang tubers contain high moisture and calcium oxalate which make them highly perishable and can cause an itching sensation (Impaprasert *et al*., 2014; Nurlela *et al*., 2021). These properties hinder direct marketing of fresh tubers due to limited storability. To address this issue, drying is a pivotal step in porang postharvest processing (Setiavani *et al*., 2025). Drying serves to reduce moisture content, extend shelf life, and facilitate distribution and downstream processing (Dar *et al*., 2022; Veena *et al*., 2023). The dried products (chips or flour) are expected to meet quality standards, notably low moisture and preserved glucomannan content. Product quality is strongly influenced by drying conditions and raw-material characteristics so that understanding the drying rate is crucial.

The drying rate is defined as the rate of water removal from a material during drying, measured by changes in moisture content over time (Rahmia *et al*., 2023; Setiavani *et al*., 2025). This parameter plays a key role in determining product quality, shelf life, and the stability of bioactive compounds (Dar *et al*., 2022; Gusmalawati, 2021; Veena *et al*., 2023). Each material exhibits distinct drying-rate characteristics depending on slice thickness, porosity, and chemical composition (Ononogbo *et al*., 2022; Rahmia *et al*., 2023; Schlünder, 2004). Prior research has addressed drying-process modelling using the Midlii, Henderson, and Chung–Pfost models (Fadila *et al*., 2023; Hawa *et al*., 2022). Comparative studies of drying methods such as oven drying, conventional drying, solar dryers, and greenhouse drying indicate that solar dryers can yield the highest drying rates and glucomannan contents (Setiavani *et al*., 2025). In addition, investigations into pretreatments and product quality have included soaking in 5% ascorbic acid for 120 minutes to enhance chip whiteness; steeping slices in acid/salt solutions to reduce calcium oxalate and alter flour viscosity; and vacuum–microwave drying, which improved colour and KGM viscosity (Impaprasert *et al*., 2014; Kumoro *et al*., 2019; Ratnawati *et al*., 2024).

Recent studies show that porang tuber drying typically follows a two-stage falling-rate pattern without a constant-rate period, in contrast to other tubers such as sweet potatoes and potatoes that still exhibit such a phase (Diamante & Munro, 1991; Susanto *et al*., 2025). This difference is primarily attributed to porang's high glucomannan content which slows surface evaporation and makes internal diffusion the dominant mechanism of moisture migration (Kapoor *et al*., 2024; Yang *et al*., 2017). Beyond chemical composition, physical aspects including tuber size, slice thickness, and harvest period have significant effects on drying efficiency, retained glucomannan content, and the quality of dried products (Amanto *et al*., 2023; Korese & Achaglinkame, 2024; Sholichah *et al*., 2023). Although many studies have examined drying methods, hybrid technologies, and pretreatments for tuber crops, research on raw-material variability linked to tuber drying behaviour remains limited. Moreover, existing studies on porang drying predominantly focus on empirical drying curves or thin-layer models, without explicitly quantifying the convective heat transfer coefficient (h) and the effective drying rate constant (k_p) through numerical solutions of coupled heat–mass balance equations.

To overcome these limitations, a mechanistic yet simple modelling framework is needed to estimate parameters that are directly relevant to the process. The Lewis drying model offers a first-order representation that can be interpreted physically for convective drying, where the effective drying rate coefficient can be associated with the combined effects of heat and mass transfer. By numerically solving the main differential form of the Lewis model using a fourth-order Runge–Kutta (RK4) approach, the convective heat transfer coefficient (h) and effective drying rate constant (k_p) can be measured. Therefore, this study aims to evaluate the effect of harvest period and tuber size on the drying rate of porang chips using an integrated heat-mass balance model solved using the fourth-order Runge-Kutta (RK4)-Lewis numerical method, which produces the effective drying rate constant (k_p) and the convective heat transfer coefficient of the drying air (h). This study proposes a Runge-Kutta-Lewis-based numerical approach to estimate the drying parameters of porang

slices, including the convective heat transfer coefficient and the effective drying rate constant. The results provide quantitative parameters that can be used to estimate the drying time and support the selection of appropriate drying conditions for porang processing.

2. MATERIALS AND METHODS

2.1. Materials and Experimental Design

The primary material in this study was three-year-old porang tubers (*Amorphophallus oncophyllus*) obtained from agricultural fields in Nglanggeran Village, Patuk, Gunungkidul, Special Region of Yogyakarta. Procurement was carried out by monthly harvesting with a yield of 50–60 kg per month. The tubers used in the experiments were harvested in 2020 across five periods (June, July, August, September, and October) and classified into three size categories (small, medium, and large). Size classes were defined using lower and upper diameter thresholds of 10 and 20 cm, respectively, yielding small ($d < 10$ cm), medium ($10 \text{ cm} \leq d \leq 20$ cm), and large ($d > 20$ cm). Examples of fresh porang tuber show in Figure 1 until Figure 3, whereas the slice porang shows in Figure 4. A completely randomized design (CRD) was employed with two factors: harvest time (five levels) and tuber size (three levels). Accordingly, there were 15 treatment combinations. For each harvest time and tuber size combination, drying was conducted in a single run. Product mass was monitored using five small trays (Figure 4) placed within the dryer as subsampling units. The statistical model for this two-factor CRD can be written as Equation (1).

$$Y_{ijk} = \mu + A_i + B_j + (AB)_{ij} + \epsilon_{ijk} \quad (1)$$

Figure 1. Small-June Fresh porang

Figure 2. Medium-June Fresh porang

Figure 3. Large-June Fresh porang

Figure 4. Porang slice on Ohaus pan resembled aluminum wire-mesh screen

where Y_{ijk} is the response of the $k^{\text{-th}}$ observation at the $i^{\text{-th}}$ harvest period and $j^{\text{-th}}$ size category (k = 1, 2, ..., 5); μ is the overall mean; A_i and B_j are the fixed main effects of harvest time and tuber size, respectively; $(AB)_{ij}$ is their interaction effect; and ϵ_{ijk} is the random error term. Data was analyzed using analysis of variance (ANOVA) at the 5% significance level. When significant effects were detected ($p < 0.05$), post hoc mean separation was performed using Duncan's Multiple Range Test (DMRT) to identify differences among treatments.

2.2. Research Methods

Healthy, pest-free, and defect-free porang tubers were used. Tubers were washed and sliced to a uniform thickness of 7 mm; the resulting slices served as the test material for drying. For each treatment, five replicate samples were prepared for mass observation and three replicate samples for material-temperature observation. Both sets used an initial sample mass of approximately 100–120 g, placed on an aluminum wire-mesh screen for drying. Drying was conducted in a cabinet dryer (Shimizu Scientific Instrument PSN-150, Japan) at a constant temperature of 50 °C. Each mass-observation sample was weighed using a bench balance (Ohaus Scout SPX2202, China) initially (t = 0) and subsequently at 1-h intervals for up to 24 h, or until a constant mass was reached, indicating moisture equilibrium. Final mass of the porang slices was determined using an analytical balance (Shimadzu AW220, Japan). The recorded mass at each interval was then used to calculate moisture content and drying rate. Product temperature was monitored on three trays at 1-h intervals using a thermocouple thermometer (Xintest HT-9815, China).

2.3. Research Parameters

In this study, observations of the drying process focused on five key parameters representing the dynamics of heat and mass transfer. These five parameters included product temperature (T_p), drying chamber temperature (T_a), initial sample mass (m_s), and dry sample mass (m_d), which were measured hourly to calculate the instantaneous moisture content. Product temperature (T_p) and air drying temperature (T_a) were recorded at 5-min intervals during the first 2 h and subsequently at 1-h intervals up to 24 h, whereas sample mass (m) was measured at 1-h intervals throughout the drying process. Temperature data recorded at 5-min intervals during the first 2 h were averaged within each hour to represent early-stage variation for RK4 fitting. For numerical modeling using the fourth-order Runge–Kutta (RK4) method, all datasets were aligned to a common hourly base corresponding to the mass measurement interval.

2.3.1. Moisture Content

The moisture content is expressed in two bases, namely wet basis (MC_{wb}) and dry basis (MC_{db}) (Widhiantari *et al.*, 2025). MC_{wb} is the ratio of water mass to wet material mass, while MC_{db} is the ratio of water mass to dry material mass. In determining moisture content, the mass of the sample is categorised into three types, including water mass (m_w), sample mass (m_s), and dry mass (m_d). The determination of water mass based on the sample mass and the dry sample mass is given in Equations (2) and (3). The equations used to determine moisture content and to convert between wet- and dry-basis moisture contents are shown in Equations (4) and (5).

$$m_w = m_s - m_d \tag{2}$$

$$MC_{wb} = \frac{m_w}{m_s} \times 100 \tag{3}$$

$$MC_{db} = \frac{m_d}{m_s} \times 100 \tag{4}$$

$$MC_{db} = \frac{MC_{wb}}{1 + MC_{wb}} \tag{5}$$

where m_w, m_s, and m_d in gram, while MC_{wb} and MC_{db} in %.

2.3.2. Drying Rate and Drying Constant

The convective heat transfer coefficient (h) and drying rate k_p are two factors that interpret the drying process: h is an indicator that shows the heat transfer value from the drying air to the outer layer of the porang sheet, k_P is an indicator that states how fast the drying process takes place. The determination of h and k_p is based on the concepts of heat balance

(Equation 6) and mass balance (Equation 7). The definition of the concept of mass balance needs to be developed. This development adapts the semi-industrial convective drying simulation of mangoes described in equation 8 (Desmorieux *et al*., 2008). To facilitate the determination of h and k_p values, the drying rate model in this study follows the Lewis model (Janjai & Bala, 2012). The Lewis drying model is shown in equation (9). To support the determination of h and kP, the specific heat of water, the heat of porang tubers, and the latent heat of water are required. The specific heat of water (C_{pa}) is assumed to be 4180 J kg^{-1} K^{-1}, the specific heat of porang tubers (C_{pp}) is assumed to follow equation 11, and the latent heat is assumed to be 2260 kJ/kg.

$$\dot{Q}_{in} = \dot{Q}_{out} \tag{6}$$

$$\dot{m}_{in} = \dot{m}_{out} \tag{7}$$

$$\frac{d(MC_{db})}{dt} = -k_d|(MC_{db}) - (MC_{db})| \tag{8}$$

$$m_d \cdot \left(\frac{d(MC_{db})}{dt}\right) = -n_v \cdot a_c \tag{9}$$

$$-n_v = \frac{m_d \cdot \left(\frac{d(MC_{db})}{dt}\right)}{a_c} \tag{10}$$

$$C_{pp} = 0.837 + 3.349 \cdot MC_{wb} \tag{11}$$

The determination of the convective heat transfer coefficient (h) and the drying rate constant (k_p) was performed using the fourth-order Runge-Kutta (RK4) approach. The determination was performed in Rstudio software by setting the lowest error value based on the Mean Absolute Percentage Error (MAPE) equation. The final derived forms of Equations (6)–(9), describing the temporal changes in material temperature and moisture content, obtained using the RK4 method are presented below.

$$\frac{dT_p}{dt} = \frac{(-k \times |MC_{db} - MC_e| \times L_v)}{(C_{pp} + C_{pa} \times MC_{db})} + \frac{\left(h \times A \times (T_a - T_p)\right)}{m_d \times (C_{pp} + C_{pa} \times MC_{db})} \tag{12}$$

$$T_{p;i+1} = T_{p;i} + \frac{1}{6} \times \left((g_1 + 2g_2 + 2g_3 + g_4)\right) \tag{13}$$

$$g_1 = \left[\frac{(-k \times |MC_{db} - MC_e| \times L_v)}{(C_{pp} + C_{pa} \times MC_{db})} + \frac{\left(h \times A \times (T_a - T_p)\right)}{m_d \times (C_{pp} + C_{pa} \times MC_{db})}\right] \times s \tag{14}$$

$$g_2 = \left[\frac{\left(-k \times \left(MC_{db} + \frac{v_1}{2} - MC_e\right) \times L_v\right)}{(C_{pp} + C_{pa} \times MC_{db})} + \frac{\left(h \times A \times \left(T_a - \left(T_p + \frac{g_1}{2}\right)\right)\right)}{m_d \times \left(C_{pp} + C_{pa} \times \left(MC_{db} + \frac{v_1}{2}\right)\right)}\right] \times s \tag{15}$$

$$g_3 = \left[\frac{\left(-k \times \left(MC_{db} + \frac{v_2}{2} - MC_e\right) \times L_v\right)}{(C_{pp} + C_{pa} \times MC_{db})} + \frac{\left(h \times A \times \left(T_a - \left(T_p + \frac{g_2}{2}\right)\right)\right)}{m_d \times \left(C_{pp} + C_{pa} \times \left(MC_{db} + \frac{v_2}{2}\right)\right)}\right] \times s \tag{16}$$

$$g_4 = \left[\frac{(-k \times (MC_{db} + v_3 - MC_e) \times L_v)}{(C_{pp} + C_{pa} \times MC_{db})} + \frac{\left(h \times A \times \left(T_a - (T_p + g_3)\right)\right)}{m_d \left(C_{pp} + C_{pa} \times (MC_{db} + v_3)\right)}\right] \times s \tag{17}$$

$$\frac{d(MC_{db})}{dt} = -k|(MC_{db}) - (MC_e)| \tag{18}$$

$$MC_{db;i+1} = MC_{db;i} + \frac{1}{6} \times \left((v_1 + 2v_2 + 2v_3 + v_4)\right) \tag{19}$$

$$v_1 = [-k|(MC_{db}) - (MC_e)|] \times s \quad (20)$$

$$v_2 = \left[-k\left|\left(MC_{db} - \frac{v_1}{2}\right) - (MC)_e\right|\right] \times s \quad (21)$$

$$v_3 = \left[-k\left|\left(MC_{db} - \frac{v_2}{2}\right) - (MC)_e\right|\right] \times s \quad (22)$$

$$v_4 = [-k|(MC_{db} - v_3) - (MC)_e|] \times s \quad (23)$$

In this derivation, the surface area of the porang slice is required. The surface area of the porang slice is determined by comparing the area of the aluminum strip to the area of the porang using Corel Draw X7 (Alludo, Canada). The surface area of the porang slice was determined from 10 sample images. Shrinkage of the porang slices during drying was assumed to be negligible; therefore, the surface area was treated as constant and represented by the average value of 127.64 cm² obtained from image analysis. The numerical solution of the coupled heat–mass balance equations based on the Lewis thin-layer model was implemented using a fourth-order Runge–Kutta (RK4) method. All numerical computations and model simulations were performed using Rstudio (Posit Software, USA).

2.4. Model Performance Evaluation

2.4.1. MAPE

MAPE (mean absolute percentage error) is a method of evaluating the accuracy of predicted values against observed values of an event. MAPE is expressed as an average of the absolute value of all percentage differences between predicted and observed values against observed values (Nabillah & Ranggadara, 2020). It is defined as Equation 24.

$$\text{MAPE} = \frac{1}{n}\sum_i^n \left|\frac{\hat{a}_i - a_i}{a_i}\right| \times 100 \quad (24)$$

In this study, MAPE values were used to determine the parameters of h and k_P. The resulting MAPE serves as an indicator of how well the candidate model equation approximates the phenomenon under study; lower MAPE values indicate better predictive performance (Meade, 1983). The interpretive categories for MAPE adopted in this work are presented in Table 1.

Table 1. MAPE interpretation for model accuracy

MAPE Interval	Interpretation
< 10%	Very high accuracy
10–20%	High accuracy
20–50%	Acceptable accuracy
> 50%	Poor accuracy

2.4.2. Two-way ANOVA

Analysis of variance (ANOVA) is a statistical analysis method used to determine the diversity of a data group (Einax, 2010). Determination of diversity is based on the calculation of the deviation value of a data set. The deviation value is determined between groups, within groups, and in total. The three types of deviation are squared and then averaged. The average of these three types of deviations is used as a standard deviation that has been generally stated to determine the significance of data diversity. Two-way analysis of variance (ANOVA) was conducted using the Data Analysis Tool-Pack in Microsoft Excel (Microsoft Corporation, USA).

3. RESULTS AND DISCUSSION

3.1. Temperature of Porang Slice

The product temperature profile (T_p) during porang drying in different harvest months and slice sizes is shown in Figure 5 until Figure 9. Based on these five graphs, the changes in product temperature (T_p) during porang drying follow the typical drying stages which are the initial period, the constant rate period, and the falling rate period (James, 2020; Zheng *et al*., 2015). During the initial period, the heat supplied to the material is mainly used to increase the product

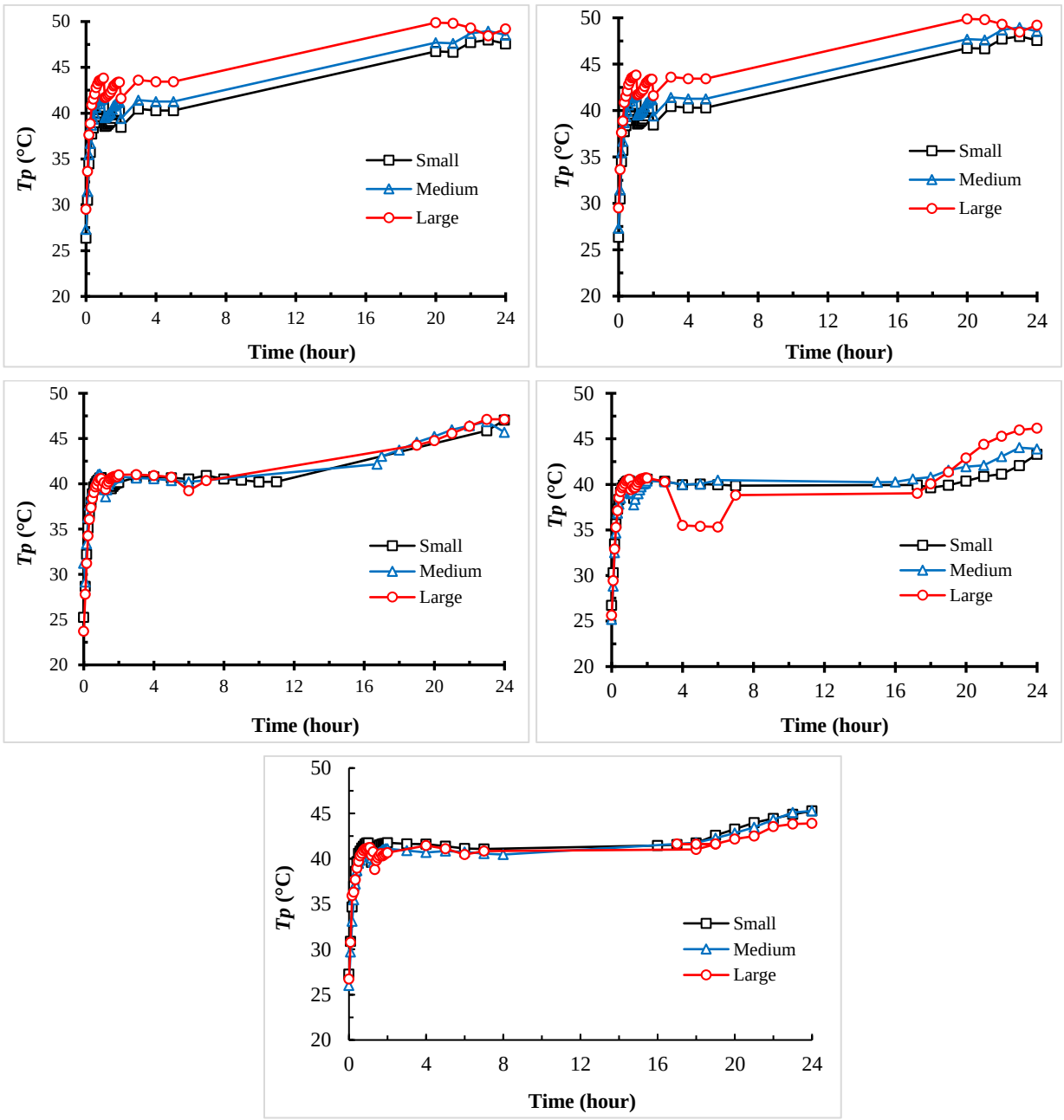

Figure 9. Product temperature (T_p) profiles of porang slices of different sizes during convective drying at 50 °C: (a) June, (b) July, (c) August, (d) September, and (e) October

temperature and cause the evaporation of free water (Hii *et al*., 2023; Masuda *et al*., 2006; Tajudin *et al*., 2019) resulting in a rapid increase in T_p from an initial range of approximately 27–30 °C to 38–42 °C in all graphs. Later, in the constant rate period, the product surface remains saturated with moisture and the transferred heat energy is mostly consumed by evaporation (Gonçalves *et al*., 2012; Tatemoto & Koda, 2023) causing the increase in T_p to proceed very slowly or remain relatively stable in the range of 39–43 °C. As the process enters the decreasing rate period, the reduction of free water on the surface and the increase in resistance to internal mass transfer cause a decrease in evaporative heat consumption allowing some of the supplied heat energy to accumulate in the material. This condition is consistently reflected in all graphs through a gradual increase in T_p towards a final temperature of approximately 44–50 °C depending on the month of harvest.

3.2. Convective Heat Transfer Rate (*h*)

Table 2 summarizes the convective heat transfer coefficient (*h*) of porang slices as affected by harvest month and tuber diameter, showing clear quantitative variation across the 15 treatment combinations. The lowest h values occurred in June, ranging narrowly between 40.11 and 44.63 $W{\cdot}m^{-2}{\cdot}°C^{-1}$ across all size classes. In contrast, October produced consistently high *h* values across sizes (63.54-83.84 $W{\cdot}m^{-2}{\cdot}°C^{-1}$), with small tubers exhibiting the highest cell values (83.84 $W{\cdot}m^{-2}{\cdot}°C^{-1}$) in that month. September showed the most pronounced within-month variation: medium tubers reached 102.13 $W{\cdot}m^{-2}{\cdot}°C^{-1}$, far above small (44.18 $W{\cdot}m^{-2}{\cdot}°C^{-1}$) and large (59.82 $W{\cdot}m^{-2}{\cdot}°C^{-1}$) tubers in the same month, while in July and August the size effect was modest and monotonic. The directional reversal of the size effect across months, with September showing an inverted pattern relative to July and October, indicates that harvest month and tuber diameter interact jointly rather than independently on h.

Table 2. Convective heat transfer coefficient of porang slices ($W{\cdot}m^{-2}{\cdot}°C^{-1}$) for variation of harvest month and tuber diameter

Porang Variation	Small	Medium	Large
June	40.11^{a}	44.63^{ab}	41.27^{a}
July	57.66^{cd}	56.53^{cd}	52.66^{bc}
August	50.48^{bc}	53.91^{c}	44.65^{ab}
September	44.18^{ab}	102.13^{g}	59.82^{cde}
October	83.84^{f}	68.27^{e}	63.54^{de}

Note: means followed by the same superscript letter are not significantly different at α = 0.05 according to Duncan's multiple range test

Table 3. Summary of two-way ANOVA on drying rate coefficient of porang slices for variation of harvest month and tuber size

Source of Variation	SS	df	MS	*F*	*P*-value	*F* crit	Interpretation
Harvest Period	9557.38	4	2389.35	55.93	< 0.001	2.53	Significant
Tuber Size	2219.52	2	1109.76	25.98	< 0.001	3.15	Significant
Harvest Period × Tuber Size	8240.23	8	1030.03	24.11	< 0.001	2.10	Significant
Error	2563.27	60	42.72				
Total	22580.4	74					

Table 3 presents the results of the two-way ANOVA assessing the effects of the harvest period, tuber size, and their interaction on the convective heat transfer coefficient (*h*) of porang slices. All three sources of variation were statistically significant at the 95% confidence level. Harvest period exerted a strong main effect on *h* ($F_{measure} = 55.93 > F_{crit} = 2.53$; $p_{value} < 0.001$) confirming that *h* values differed systematically across the five harvest months. Tuber size also produces a significant main effect ($F_{measure} = 25.98 > F_{crit} = 3.15$; $p_{value} < 0.001$) indicating that small, medium, and large slices were not interchangeable in terms of convective heat transfer behaviour. The harvest period × tuber size interaction was likewise highly significant ($F_{measure} = 24.11 > F_{crit} = 2.10$l; $p_{value} < 0.001$) demonstrating that the influence of one factor on *h* depended on the level of the other. Because the interaction was significant, the cell-level comparison in Table 2 (rather than the marginal main effects) provide the appropriate basis for interpretation.

The significant effects of harvest period, tuber size, and their interaction on *h* reflect the combination contribution of process dynamics and material properties of porang slices. Drying-process conditions shape *h* through the air-product temperature gradient, airflow distribution, and progressive modification of product surface characteristics as moisture is removed (Kalantari *et al*., 2023; Zhu, 2018; Zhu *et al*., 2020). These conditions remain sensitive to the initial physical and chemical state of the slice. Material properties of porang tissue, in particular the effective thermal conductivity and internal moisture distribution, govern the local heat and mass transfer response (Božiková *et al*., 2017; Mehrali *et al*., 2015; Wang *et al*., 2020). The significant tuber size main effect is consistent with the geometric scaling of surface-area-to-volume ratio that modulates convective exchange between the slice and the surrounding air (Mehrali *et al*., 2015). The significant harvest period main effect aligns with seasonal variation in tuber composition. Glucomannan content and water-binding capacity in *Amorphophallus* corms shifts across vegetative growth stages (Chua *et al*., 2013). The significant interaction further indicates that the size-dependent geometric response is modulated by the harvest-stage composition of the tuber, plausibly through differences in initial moisture content and glucomannan-mediated diffusion

resistance during the early drying phase (Huang *et al*., 2002; Yang *et al*., 2017). The anomalously high *h* value observed for medium-size tubers in September (102.13 $W \cdot m^{-2} \cdot °C^{-1}$) likely reflects a transitional physiological state at the onset of dormancy and warrants cautious interpretation. Consequently, treatment-specific *h* values rather than a single global average should be adopted when accurate drying-process design is required.

3.3. Effective Drying Rate Constant (k_p)

Table 4 presents the drying rate coefficient (k_p) of porang slices as influenced by harvest month and tuber diameter showing substantial cell-to-cell variation across the 15 treatment combinations. The highest k_p was observed in July small slices (4.34 h^{-1}), while the lowest k_p was observed in October large slice (2.32 h^{-1}). The size-dependent pattern in within each month is not uniform across months. In June, k_p increased monotonically with tuber size reaching 3.10 h^{-1} in small slices, 3.48 h^{-1} in medium slices, and 4.06 h^{-1} in large slices. In October, the opposite trend was observed with k_p decreasing to 3.02 h^{-1} in small slices, 2.76 h^{-1} in medium slices, and 2.32 h^{-1} in large slices. In contrast, August and September departed from both monotonic patterns. August showed the lowest k_p in medium slices (2.54 h^{-1}), producing a U-shaped pattern across tuber size. September showed a sharp jump only at the large size class with k_p reached 3.74 h^{-1} while small and medium slices clustered near 2.48 to 2.58 h^{-1}. The collective pattern across all five harvest months, with distinct trends in both direction and magnitude, indicates that the size effect on k_p cannot be summarized by a single averaged trend. This finding confirms that harvest month and tuber size interact jointly on the drying-rate response.

Table 4. Drying rate coefficient (h^{-1}) of porang slices for variation of harvest month and tuber diameter

Harvest Period	Small	Medium	Large
June	3.1^{de}	3.48^{efg}	4.06^{hi}
July	4.34^{i}	3.64^{fgh}	3.98^{hi}
August	2.86^{bcd}	2.54^{abc}	3.2^{def}
September	2.48^{ab}	2.58^{abc}	3.74^{ghi}
October	3.02^{cde}	2.76^{abcd}	2.32^{a}

Note: means followed by the same superscript letter are not significantly different at α = 0.05 according to Duncan's multiple range test

Table 5. Summary of two-way ANOVA on drying rate coefficient of porang slices for variation of harvest month and tuber size

Source of Variation	SS	df	MS	*F*	*P*-value	*F* crit	Interpretation
Harvest Period	17.57	4	4.39	35.84	< 0.001	2.53	Significant
Tuber Size	2.73	2	1.36	11.13	< 0.001	3.15	Significant
Harvest Period × Tuber Size	8.08	8	1.01	8.25	< 0.001	2.10	Significant
Error	7.35	60	0.12				
Total	35.73	74					

Table 5 reports the two-way ANOVA evaluating the effects of harvest period, tuber size, and their interaction on the drying rate coefficient (k_p) of porang slices. Each of the three variation sources reached statistical significance at 95% confidence level. Harvest period yielded a strong main effect on k_p ($F_{measure} = 35.84 > F_{crit} = 2.53$; $p_{value} < 0.001$), indicating systematic differences in k_p across the five harvest months. A significant main effect of tuber size was also detected ($F_{measure} = 11.13 > F_{crit} = 3.15$; $p_{value} < 0.001$), showing that k_p depended on the slice size class. The interaction term between harvest period and tuber size was likewise significant ($F_{measure} = 8.25 > F_{crit} = 2.10$; $p_{value} < 0.001$), demonstrating that the effect of one factor on k_p varied with the level of the other. This significant interaction provides the statistical foundation for the contrasting size-dependent patterns observed across June, October, August, and September in Table 4, rather than the per-factor averages constitute the appropriate unit of inference.

The significant main effects and interaction observed for k_p can be linked to specific mechanistic factors via existing literature on tuber drying and *Amorphophallus* physiology. For the harvest period main effect, compositional shifts in the corm during vegetative growth and post-harvest storage are presumed to alter the drying-rate response. Previous physiological and metabolomic studies indicate that the carbohydrate composition and glucomannan-derived properties of *Amorphophallus* tubers vary across growth stages and processing-related modifications (Aanisah *et al*., 2022; Chua *et al*., 2013; Gusmalawati, 2021). For the tuber size main effect, the surface-area-to-volume ratio is presumed to drive

geometric scaling of the diffusion path within each slice. The drying rate is sensitive to slice thickness and porosity, as documented for tubers and root crops such as sweet potato and taro (Gasa *et al*., 2022; Molla *et al*., 2023). For the interaction, the compositional shifts at each harvest stage are presumed to modulate the diffusion behaviour of the glucomannan-rich tissue, plausibly through differences in initial moisture content and gel network development. Glucomannan readily forms a gel network that enhances water retention. The progressive formation of this network shifts the control of drying toward internal diffusion (Huang *et al*., 2002; Ji *et al*., 2017; Yang et al., 2017). The range of h obtained across months and sizes falls within the literature envelope of 10 to 80 $W \cdot m^{-2} \cdot °C^{-1}$ reported for food slices (Ratti & Crapiste, 1995) confirming that the inferred k_p values are physically reasonable. Accordingly, while effective average values of k_p may suffice for first-pass drying-process design, accurate scale-up should rely on treatment-specific k_p values. Controlled operating conditions of temperature and airflow remain critical to preserve product quality.

Model performance was evaluated by comparing the observed experimental drying data with the predicted values generated by the RK4-Lewis model. In this context, the observed values refer to the experimentally measured moisture-content dan temperature data at each observation time, whereas the predicted values refer to the corresponding values calculated by the RK4-Lewis model using the optimized h and k_p parameters. The MAPE values obtained across the treatment combinations ranged from 22.37% to 38.05% with an average value of 30.72%. Based on the accuracy classification used in this study, these values fall within acceptable accuracy category. Therefore, the RK4-Lewis model can be considered adequate for estimating effective drying parameters in this study.

4. CONCLUSION

This study successfully modelled the drying behaviour of porang slices (7 mm) in a 50 °C cabinet dryer using a coupled heat–mass balance integrated with the Lewis thin-layer model, numerically solved by a fourth-order Runge–Kutta method, yielding key process parameters in the form of the convective heat transfer coefficient (h) and the drying rate constant (k_p) based on MAPE goodness-of-fit criteria. The product temperature profiles exhibited rapid heating to approximately 43–46 °C, followed by a more gradual increase, which is consistent with the progressive weakening of evaporative cooling at low moisture contents and confirms the predominance of the falling-rate drying regime over most of the drying duration. The estimated h values ranged from approximately 42 $W \cdot m^{-2} \cdot °C^{-1}$ in June to 72 $W \cdot m^{-2} \cdot °C^{-1}$ in October. The estimated k_p values varied between 2.70 and 4.77 h^{-1}, with higher values generally observed during June and July and lower values during August to October. Harvest period, tuber size, and their interaction all exerted statistically significant effects on both h and k_p at the 95% confidence level. Practically, effective average values of h and k_p may suffice for first-pass drying-process design, while accurate scale-up should rely on treatment-specific parameter values to preserve the functional and visual quality of porang chips. From a product quality perspective, the dominance of the falling-rate drying regime and the moderate product temperature range observed in this study suggest that moisture removal is primarily governed by internal diffusion, which is critical for preserving the functional properties of porang, particularly its glucomannan-rich matrix.

Future work should prioritize physicochemical characterization of porang tubers and their derived flour across harvest periods and tuber-size categories to determine whether variations in moisture content, glucomannan content, water-binding capacity, porosity, color, and rehydration behavior are associated with the treatment-specific h and k_p values obtained in this study.

AUTHOR CONTRIBUTION STATEMENT

Author	C	M	So	Va	Fo	I	R	D	O	E	Vi	Su	P	Fu
SA			✓		✓	✓		✓	✓	✓	✓			
SR	✓	✓	✓	✓			✓					✓		✓
EH	✓			✓								✓		
FNF						✓								
LAG									✓		✓		✓	✓

C: Conceptualization
M: Methodology
So: Software
Va: Validation
Fo: Formal Analysis
I: Investigation
D: Data Curation
R: Resources
O: Writing - Original Draft
E: Writing - Review & Editing
Vi: Visualization
Su: Supervision
Fu: Funding Acquisition
P: Project Administration

REFERENCES

Aanisah, N., Wardhana, Y.W., Chaerunisaa, A.Y., & Budiman, A. (2022). Review on modification of glucomannan as an excipient in solid dosage forms. *Polymers*, ***14***(13), 2550. https://doi.org/10.3390/polym14132550

Amanto, B.S., Chairunisa, H.O., Prabawa, S., Kawiji, & Yudhistira, B. (2023). The effect of different drying methods and slice thickness on the quality of porang (*Amorphophallus muelleri*) chips. *Jurnal Ilmiah Rekayasa Pertanian dan Biosistem*, 1***1***(2), 256–269. https://doi.org/10.29303/jrpb.v11i2.276

Bahlawan, Z.A.S., Damayanti, A., Megawati, Cahyari, K., Andriani, N., & Hapsari, R.A. (2021). Study of glucomannan extraction with hydrochloric acid catalyst and alcohol solvent based on porang tuber flour (*Amorphophallus oncophyllus*). *IOP Conference Series: Earth and Environmental Science*, ***700***(1), 012069. https://doi.org/10.1088/1755-1315/700/1/012069

Božiková, M., Híreš, Ľ., Valach, M., Malínek, M., & Mareček, J. (2017). Basic thermal parameters of selected foods and food raw materials. *Acta Universitatis Agriculturae et Silviculturae Mendelianae Brunensis*, ***65***(2), 391–400. https://doi.org/10.11118/actaun201765020391

Chua, M., Hocking, T.J., Chan, K., & Baldwin, T.C. (2013). Temporal and spatial regulation of glucomannan deposition and mobilization in corms of *Amorphophallus konjac* (Araceae). *American Journal of Botany*, ***100***(2), 337–345. https://doi.org/10.3732/ajb.1200547

Cruz, N.de.D.da, Azrianingsih, R., & da Costa, H.R. (2024). Morphological characteristics of porang (*Amorphophallus muelleri* Blume) in Timor-Leste and their correlation with the climatic conditions: *Amorphophallus muelleri* Blume in Timor-Leste. *Journal of Tropical Life Science*, ***14***(3). https://doi.org/10.11594/jtls.14.03.20

Dar, B.N., Shah, M.A., & Mir, S.A. (2022). *Shelf Life and Food Safety* (1st ed.). CRC Press. https://doi.org/10.1201/9781003091677

Desmorieux, H., Diallo, C., & Coulibaly, Y. (2008). Operation simulation of a convective and semi-industrial mango dryer. *Journal of Food Engineering*, ***89***(2), 119–127. https://doi.org/10.1016/j.jfoodeng.2008.04.007

Diamante, L.M., & Munro, P.A. (1991). Mathematical modelling of hot air drying of sweet potato slices. *International Journal of Food Science & Technology*, ***26***(1), 99–109. https://doi.org/10.1111/j.1365-2621.1991.tb01145.x

Einax, J.W. (2010). Stephen L.R. Ellison, Vicki J. Barwick, Trevor J. Duguid Farrant: Practical statistics for the analytical scientist. A bench guide, 2nd ed. *Analytical and Bioanalytical Chemistry,* ***397***(2), 409–410. https://doi.org/10.1007/s00216-010-3519-9

Fadila, Muhidong, J., & Salim, I. (2023). Isothermic model of porang tuber (*Amorphophallus muelleri* B) flour. *IOP Conference Series: Earth and Environmental Science*, ***1230***(1), 012173. https://doi.org/10.1088/1755-1315/1230/1/012173

Gasa, S., Sibanda, S., Workneh, T.S., Laing, M., & Kassim, A. (2022). Thin-layer modelling of sweet potato slices drying under naturally-ventilated warm air by solar-venturi dryer. *Heliyon*, ***8***(2), e08949. https://doi.org/10.1016/j.heliyon.2022.e08949

Gonçalves, T.D., Brito, V., & Pel, L. (2012). Water vapor emission from rigid mesoporous materials during the constant drying rate period. *Drying Technology*, ***30***(5), 462–474. https://doi.org/10.1080/07373937.2011.647184

Gusmalawati, D. (2021). Determination of postharvest quality of porang (*Amorphophallus muelleri* Blume) tubers based on the dynamics of weight loss, water content and carbohydrate components for the pharmaceutical industry. *Farmacia*, ***69***(6), 1145–1152. https://doi.org/10.31925/farmacia.2021.6.19

Handayani, S.M., Widadie, F., Rahayu, E.S., Irianto, H., Setyowati, Sundari, M.T., & Rachmanto, F. (2024). Analysis of added value and market share in porang value chain in wonogiri regency. *IOP Conference Series: Earth and Environmental Science*, ***1362***(1), 012010. https://doi.org/10.1088/1755-1315/1362/1/012010

Hawa, L.C., Septiyanto, F.G., Yulianingsih, R., Susilo, B., Lastriyanto, A., Sumarlan, S.H., Tihardo, Y., & Sinambela, L.G. (2022). Drying kinetics of porang (*Amorphophallus mueller* B.) chips under open sun drying. *IOP Conference Series: Earth and Environmental Science*, ***1038***(1), 012071. https://doi.org/10.1088/1755-1315/1038/1/012071

Hii, C.L., Chiang, C.L., & Putranto, A. (2023). Modelling heat and mass transfer processes during drying: Empirical, theoretical and reaction engineering approach. *AIP Conference Proceedings*, ***2586***, 060011. https://doi.org/10.1063/5.0105710

Huang, L., Takahashi, R., Kobayashi, S., Kawase, T., & Nishinari, K. (2002). Gelation behavior of native and acetylated konjac glucomannan. *Biomacromolecules*, ***3***(6), 1296–1303. https://doi.org/10.1021/bm0255995

Impaprasert, R., Borompichaichartkul, C., & Srzednicki, G. (2014). A new drying approach to enhance quality of konjac glucomannan extracted from *Amorphophallus muelleri*. *Drying Technology*, ***32***(7), 851–860. https://doi.org/10.1080/07373937.2013.871728

James, C.B. (2020). Drying. In *Breakfast Cereals and How They Are Made*. Elsevier. https://doi.org/10.1016/C2017-0-04647-5

Janjai, S., & Bala, B.K. (2012). Solar drying technology. *Food Engineering Reviews*, ***4***(1), 16–54. https://doi.org/10.1007/s12393-011-9044-6

Ji, L., Xue, Y., Feng, D., Li, Z., & Xue, C. (2017). Morphology and gelation properties of konjac glucomannan: Effect of microwave processing. *International Journal of Food Properties*, ***20***(12), 3023–3032. https://doi.org/10.1080/10942912.2016.1270962

Kalantari, D., Naji-Tabasi, S., Kaveh, M., Azadbakht, M., Majnooni, M., Khorshidi, Y., Asghari, A., & Khalife, E. (2023). Drying kinetics and shrinkage rate of thin‐sliced pears in different drying stages. *Journal of Food Process Engineering*, ***46***(3), e14264. https://doi.org/10.1111/jfpe.14264

Kapoor, D.U., Sharma, H., Maheshwari, R., Pareek, A., Gaur, M., Prajapati, B.G., Castro, G.R., Thanawuth, K., Suttiruengwong, S., & Sriamornsak, P. (2024). Konjac glucomannan: A comprehensive review of its extraction, health benefits, and pharmaceutical applications. *Carbohydrate Polymers*, ***339***, 122266. https://doi.org/10.1016/j.carbpol.2024.122266

Korese, J.K., & Achaglinkame, M.A. (2024). Convective drying of Gardenia erubescens fruits: Effect of pretreatment, slice thickness and drying air temperature on drying kinetics and product quality. *Heliyon*, ***10***(4), e25968. https://doi.org/10.1016/j.heliyon.2024.e25968

Kumoro, A.C., Amyranti, M., Retnowati, D.S., & Ratnawati, R. (2019). Browning prevention of chips from freshly harvested porang (*Amorphophallus oncophyllus*) tubers through immersion in ascorbic acid solutions at various times. *Journal of Physics: Conference Series*, ***1295***(1), 012023. https://doi.org/10.1088/1742-6596/1295/1/012023

Masuda, H., Higashitani, K., & Yoshida, H. (Eds.). (2006). 10 Drying. In *Powder Technology Handbook* (0 ed., pp. 649–656). CRC Press. https://doi.org/10.1201/9781439831885-55

Meade, N. (1983). Industrial and business forecasting methods, Lewis, C.D., Borough Green, Sevenoaks, Kent: Butterworth, 1982. Price: £9.25. Pages: 144. *Journal of Forecasting*, ***2***(2), 194–196. https://doi.org/10.1002/for.3980020210

Mehrali, M., Sadeghinezhad, E., Rosen, M.A., Latibari, S.T., Mehrali, M., Metselaar, H.S.C., & Kazi, S.N. (2015). Effect of specific surface area on convective heat transfer of graphene nanoplatelet aqueous nanofluids. *Experimental Thermal and Fluid Science*, ***68***, 100–108. https://doi.org/10.1016/j.expthermflusci.2015.03.012

Molla, E.T., Teka, T.A., & Taye, A.H. (2023). Effects of solar tunnel drying zones and slice thickness on the drying characteristics of taro (*Colocasia esculenta* (L.) Schott) slice. *Food Science & Nutrition*, ***11***(3), 1178–1186. https://doi.org/10.1002/fsn3.3175

Nabillah, I., & Ranggadara, I. (2020). Mean absolute percentage error untuk evaluasi hasil prediksi komoditas laut. *JOINS (Journal of Information System)*, ***5***(2), 250–255. https://doi.org/10.33633/joins.v5i2.3900

Novitasari, E., Yuniwati, I., & Kustiari, T. (2024). Development of industrial-scale Porang tuber flouring machine in Banyuwangi. *AIP Conference Proceedings*, ***3222***, 050011. https://doi.org/10.1063/5.0231289

Nurkhamidah, S., Heksa, A.C., Widjaja, T., Ni'mah, H., & Wardhono, E. (2024). One-step ethanol extraction for producing purified glucomannan flour from porang chips (*Amorphophallus oncophyllus*). *ASEAN Engineering Journal*, ***14***(3), 169–174. https://doi.org/10.11113/aej.v14.21391

Nurlela, N., Ariesta, N., Laksono, D.S., Santosa, E., & Muhandri, T. (2021). Characterization of glucomannan extracted from fresh porang tubers using ethanol technical grade. *Molekul*, ***16***(1), 1. https://doi.org/10.20884/1.jm.2021.16.1.632

Nurmianto, E., Anzip, A., & Kusrini, D.E. (2020). An ergonomic, mobile and portable design of porang cutting and drying machine on motorcycle. *IOP Conference Series: Materials Science and Engineering*, ***722***(1), 012075. https://doi.org/10.1088/1757-899X/722/1/012075

Ononogbo, C., Nwakuba, N.R., Nwaji, G.N., Nwufo, O.C., Nwosu, E.C., Okoronkwo, C.A., Igbokwe, J.O., & Anyanwu, E.E. (2022). Thermal efficiency and drying behaviour of yam slices in a dryer driven by the waste heat of exhaust gases. *Scientific African,* ***17***, e01310. https://doi.org/10.1016/j.sciaf.2022.e01310

Rahmia, S., Muhidong, J., Salengke, & Laga, A. (2023). Passive drying of Porang (*Amorphophallus oncophylus*) slices. *AIP Conference Proceedings*, ***2596***, 050001. https://doi.org/10.1063/5.0119980

Ratnawati, L., Indrianti, N., Afifah, N., Ekafitri, R., Sholichah, E., Desnilasari, D., Setiaboma, W., Kristanti, D., & Sarifudin, A. (2024). Effect of soaking treatments in acid and salt solutions on physicochemical, structural, thermal and rheological properties of porang. *Food Technology and Biotechnology*, ***62***(4), 512–524. https://doi.org/10.17113/ftb.62.04.24.8503

Ratti, C., & Crapiste, G.H. (1995). Determination of heat transfer coefficients during drying of foodstuffs. *Journal of Food Process Engineering*, ***18***(1), 41–53. https://doi.org/10.1111/j.1745-4530.1995.tb00353.x

Schlünder, E.-U. (2004). Drying of porous material during the constant and the falling rate period: A critical review of existing

hypotheses. *Drying Technology*, ***22***(6), 1517–1532. https://doi.org/10.1081/DRT-120038738

Setiavani, G., Devita, L., & Sari, M. (2025). The effect of drying method on physical and chemical characterictic of porang (*Amorphophallus muelleri* Blume) chips in North Sumatera Province. *BIO Web of Conferences*, ***158***, 04008. https://doi.org/10.1051/bioconf/202515804008

Sholichah, E., Purwono, B., Murdiati, A., Syoufian, A., & Sarifudin, A. (2023). Extraction of glucomannan from porang (*Amorphophallus muelleri* Blume) with freeze-thaw cycles pre-treatment. *Food Science and Technology*, ***43***. https://doi.org/10.5327/fst.1423

Soedarjo, M. (2021). Effect of bulbil sizes on growth and corm yield of porang (*Amorphophallus muelleri* Blume) grown on alfisol soil. *IOP Conference Series: Earth and Environmental Science*, ***733***(1), 012079. https://doi.org/10.1088/1755-1315/733/1/012079

Soemantri, A. S., Kamsiati, E., & Herawati, H. (2021). Analysis of added value on the porang supply chain in Klangon Village, Madiun District. *IOP Conference Series: Earth and Environmental Science*, ***892***(1), 012039. https://doi.org/10.1088/1755-1315/892/1/012039

Susanto, E. E., Saptoro, A., Kumar, P., Tiong, A.N.T., Putranto, A., & Suherman, S. (2025). 7E + Q analysis of a novel modified mixed-mode solar dryer for porang chips. *Drying Technology*, ***43***(5), 858–877. https://doi.org/10.1080/07373937.2025.2473564

Tajudin, N.H.A., Tasirin, S.M., Ang, W.L., Rosli, M.I., & Lim, L.C. (2019). Comparison of drying kinetics and product quality from convective heat pump and solar drying of Roselle calyx. *Food and Bioproducts Processing*, ***118***, 40–49. https://doi.org/10.1016/j.fbp.2019.08.012

Tatemoto, Y., & Koda, Y. (2023). Evaluation of the constant drying rate of organic solvents using a liquid supply method. *Drying Technology*, ***41***(15), 2476–2486. https://doi.org/10.1080/07373937.2023.2255272

Veena, N., Goyal, M.R., & Watharkar, R.B. (2023). *Novel and Alternative Methods in Food Processing: Biotechnological, Physicochemical, and Mathematical Approaches* (1st ed.). Apple Academic Press. https://doi.org/10.1201/9781003328605

Wahidah, B.F., Afiati, N., & Jumari, J. (2021). Community knowledge of *Amorphophallus muelleri* Blume: Cultivation and utilization in Central Java, Indonesia. *Biodiversitas Journal of Biological Diversity*, ***22***(7). https://doi.org/10.13057/biodiv/d220722

Wang, Z., Han, F., Li, Y., & Sundén, B. (2020). Numerical investigation on thermal performance design of cryogenic compact heat exchangers with serrated-fin channels. *Heat Transfer Engineering*, ***41***(22), 1856–1868. https://doi.org/10.1080/01457632.2019.1674554

Widhiantari, I.A., Sukmawaty, S., Murad, M., Arrohman, M.Y., Sandhiyana, A.B., & Gunawan, G. (2025). Drying characteristics of cayenne pepper (*Capsicum frutescens* L.) using a rotary rack hybrid dryer with blanching pretreatment application. *Jurnal Teknik Pertanian Lampung (Journal of Agricultural Engineering)*, ***14***(3), 1085-1097. https://doi.org/10.23960/jtep-l.v14i3.1085-1097

Yang, D., Yuan, Y., Wang, L., Wang, X., Mu, R., Pang, J., Xiao, J., & Zheng, Y. (2017). A review on konjac glucomannan gels: Microstructure and application. *International Journal of Molecular Sciences*, ***18***(11), 2250. https://doi.org/10.3390/ijms18112250

Zheng, X., Fu, N., Duan, M., Woo, M. W., Selomulya, C., & Chen, X. D. (2015). The mechanisms of the protective effects of reconstituted skim milk during convective droplet drying of lactic acid bacteria. *Food Research International*, ***76***(3), 478–488. https://doi.org/10.1016/j.foodres.2015.07.045

Zhu, A. (2018). The convective hot air drying of *Lactuca sativa* slices. *International Journal of Green Energy*, ***15***(3), 201–207. https://doi.org/10.1080/15435075.2018.1434523

Zhu, A., Zhao, J., & Wu, Y. (2020). Modeling and mass transfer performance of *Dioscorea alata* L. slices drying in convection air dryer. *Journal of Food Process Engineering*, ***43***(7), e13427. https://doi.org/10.1111/jfpe.13427